Effect of lithium trifluoromethanesulfonate on the phase diagram of a liquid-crystalline amphiphilic diblock copolymer

Takeshi Yamada,[a] Jingze Li,[b,c] Chinami Koyanagi,[c] Tomokazu Iyoda[b,c] and Hirohisa Yoshida[d,c]*

[a]Graduate School of Engineering, Tokyo Metropolitan University, Japan, [b]Chemical Resources Laboratory, Tokyo Institute of Technology, Japan, [c]CREST-JST, Japan, and [d]Faculty of Urban Environmental Science, Tokyo Metropolitan University, Japan. Correspondence e-mail: yoshida-hirohisa@c.metro-u.ac.jp

Phase transitions and nanometre-scale ordered structures of a binary system of a liquid-crystalline amphiphilic diblock copolymer, poly(ethylene oxide)-b-poly{11-[4-(4-butylphenylazo)phenoxy]undecyl methacrylate} [PEO_m-b-$PMA(Az)_n$, where m and n are the degrees of polymerization of the PEO and PMA(Az) domains, respectively], and lithium trifluoromethanesulfonate ($LiCF_3SO_3$) were investigated by differential scanning calorimetry and small-angle X-ray scattering (SAXS). PEO_{114}-b-$PMA(Az)_{51}$ formed a highly ordered hexagonally packed PEO cylinder structure in the temperature range below 393 K and transformed to a body-centred-cubic structure in the isotropic state above 393 K. The PEO_{114}-b-$PMA(Az)_{51}$/$LiCF_3SO_3$ systems with various $LiCF_3SO_3$ concentrations (molar ratio $0 < LiCF_3SO_3/EO = f_{Li} < 1$) formed the hexagonally packed cylinder structure at room temperature. From the effects of $LiCF_3SO_3$ concentration on the phase transitions, the size and the order of the hexagonally packed cylinder structure, it was found that PEO_{114}-b-$PMA(Az)_{51}$ and $LiCF_3SO_3$ formed a complex efficiently at a molar equivalent of three ethylene oxide repeating units per $LiCF_3SO_3$ unit. The ordering of the hexagonally packed cylinder structure decreased with increasing $LiCF_3SO_3$ concentration and the radius of the PEO cylinder evaluated by SAXS profile fitting increased from 2.7 to 8.3 nm. For the PEO_{114}-b-$PMA(Az)_{51}$/$LiCF_3SO_3$ system with $f_{Li} = 1$, the hexagonally packed cylinder structure remained even in the isotropic state because the PEO volume fraction (ϕ_{PEO}) increased from $\phi_{PEO} = 0.06$ ($f_{Li} = 0$) to $\phi_{PEO} = 0.23$ ($f_{Li} = 1$) on the formation of the $LiCF_3SO_3$/PEO complex.

1. Introduction

Nanometre-scale electron-conducting materials have been paid much attention because they are expected to provide a breakthrough in lithography limits. These materials are also interesting in terms of special physical properties like quantum size effects. Block copolymers are used as templates for making nanoscale objects in many studies (Lazzari & López-Quintela, 2003) because they can provide various nanoscale ordered structures which are easily modified by changing their fractions, degree of polymerization and chemical structures (Hamley, 1998).

There are various methods for analyzing nanostructures, e.g. atomforce microscopy (AFM), transmission and scanning electron microscopies (TEM and SEM) and small-angle scattering (SAS), which have different advantages. SAS is a powerful tool for analyzing average structures of materials because the irradiated volume is much larger than the measurement area for AFM or TEM (Hamley & Castelletto, 2004). Other advantages of SAS are that it can be used for various samples such as liquids, solutions, films, powders or supercritical fluids (Arai et al., 2003) and can be coupled with various fields, for instance, temperature (Yoshida et al., 1995), pressure (Kawabata et al., 2004), magnetic, mechanical and shear fields (Kato et al., 2004). Many numerical analysis methods for analyzing SAS data for micelle solutions (Lemmich et al., 1996) and block copolymers (Hashimoto et al., 1994) have also been reported. The combination of the use of brilliant synchrotron X-radiation with thermal analysis makes it possible to analyze the dynamics of phase transitions for organic and polymeric materials (Yamada et al., 2005).

Recently we reported the syntheses of liquid-crystalline amphiphilic diblock copolymers, poly(ethylene oxide)-b-poly{11-[4-(4-butylphenylazo)phenoxy]undecyl methacrylate} [PEO_m-b-$PMA(Az)_n$, where m and n are the degrees of polymerization of the PEO and PMA(Az) domains, respectively] (Tian et al., 2002). PEO_m-b-$PMA(Az)_n$ copolymers (Fig. 1) form a highly ordered hexagonally packed PEO cylinder structure selectively over a wide range of volume fraction because the liquid crystallinity of the PMA(Az) domains stabilizes a cylinder structure rather than a sphere structure (Yoshida et al., 2004). We also reported the nanometre-size control of the hexagonally packed cylinder structure of PEO_m-b-$PMA(Az)_n$ by blending a PEO homopolymer (Jung et al., 2005) and PEO_m-b-$PMA(Az)_n$ (Jung & Yoshida, 2006).

Table 1
Characteristics of the samples studied.

f_{Li} is the molar ratio of $LiCF_3SO_3$ to a repeating unit of PEO. a, $\Delta a/a$, R, C and ϕ_{PEO} are the hexagonal lattice constant, the paracrystal distortion, the radius of a PEO cylinder, the coefficient including electron density difference and the relative PEO volume fraction estimated by SAXS profile fitting.

f_{Li}	f_{Li}^{-1}	a (nm)	$\Delta a/a$	R (nm)	C	ϕ_{PEO}
0	—	21.3	0.134	2.7	169	0.06
8.3×10^{-3}	120	21.7	0.194	2.8	44	0.06
2.5×10^{-2}	40	23.4	0.149	3.6	76	0.09
5.0×10^{-2}	20	23.6	0.179	3.8	81	0.09
1.3×10^{-1}	8	26.6	0.246	6.2	346	0.19
2.5×10^{-1}	4	28.9	0.216	7.0	1151	0.21
1.0	1	31.1	0.174	8.3	1250	0.26

PEO has potential as an electron-conducting material because it forms complexes with alkali metal ions (Rhodes & Frech, 2001). Since PEO–metal ion complexes have ionic conductivity in the solid state, they have been investigated as polymer electrodes in rechargeable batteries (Tominaga *et al.*, 2003). The combination of an anisotropic nanometre-scale structure of block copolymers and PEO–metal ion complexes is expected to produce new ionic conductive materials. We have reported the anisotropic ionic conductivity of the PEO_m-b-$PMA(Az)_n$ complex with lithium trifluoromethanesulfonate ($LiCF_3SO_3$) (Li *et al.*, 2005). The structure and the phase transitions of the PEO_m-b-$PMA(Az)_n$ complex with $LiCF_3SO_3$ are also important in considering the anisotropic conductivity. In this study, the effects of $LiCF_3SO_3$ on the phase diagram of PEO_{114}-b-$PMA(Az)_{51}$ were investigated by differential scanning calorimetry (DSC) and small-angle X-ray scattering (SAXS).

2. Samples and experiments

2.1. Samples

PEO_{114}-b-$PMA(Az)_{51}$ copolymer was synthesized by atomic transfer radical polymerization as reported elsewhere (Tian *et al.*, 2002). The molecular weight dispersion was 1.23 determined by gel permeation chromatography. $LiCF_3SO_3$ supplied from Aldrich was used without further purification. $LiCF_3SO_3$ and PEO_{114}-b-$PMA(Az)_{51}$ were dissolved in distilled tetrahydrofuran separately. Then an appropriate amount of $LiCF_3SO_3$ solution was added to the PEO_{114}-b-$PMA(Az)_{51}$ solution. The mixed solution was stirred at room temperature for 6 h. After removing the solvent, the complex samples were annealed at 413 K for 16 h and cooled down to room temperature. The $LiCF_3SO_3$ concentration is indicated by the molar ratio of $LiCF_3SO_3$ to one repeating unit of PEO, $LiCF_3SO_3/EO = f_{Li}$. The f_{Li} range in this study was from 0 to 1 (Table 1).

2.2. Experiments

2.2.1. Differential scanning calorimetry. DSC measurements were performed using a DSC 6200 calorimeter (Seiko Instruments Inc.) equipped with an electric cooling control apparatus (Haake EK90/MT) over the temperature range between 223 and 473 K. The scanning rate was 10 K min^{-1} in a nitrogen flow atmosphere
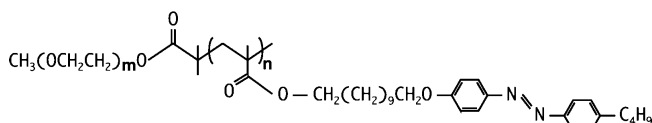
Figure 1
Chemical structure of the PEO_m-b-$PMA(Az)_n$ copolymer.

(40 ml min^{-1}) and the sample weight used for the DSC was about 3 mg.

2.2.2. Small-angle X-ray scattering. SAXS measurements were performed using the synchrotron X-radiation facility of the 2.5 GeV storage ring at BL-10C at the Photon Factory, High Energy Accelerator Research Organization (Tsukuba, Japan). Monochromatic X-rays with a wavelength λ of 0.1488 nm selected by double Si crystals were used for SAXS measurements. Two kinds of optics which covered $0.1 < q < 3$ nm^{-1} and $0.06 < q < 1.5$ nm^{-1} were used, where $q = (4\pi/\lambda)\sin\theta$ and θ is half of the diffraction angle. SAXS profiles at various temperatures were obtained using the simultaneous DSC instrument (Yoshida *et al.*, 1995). Powder samples were covered with thin aluminium foil and put in an aluminium vessel. The exposure time was 60–300 s.

3. Results and discussion

3.1. Phase transitions

Fig. 2 shows DSC heating curves for the $LiCF_3SO_3/PEO_{114}$-b-$PMA(Az)_{51}$ systems with various f_{Li}. In the case of PEO_{114}-b-$PMA(Az)_{51}$ ($f_{Li} = 0$), four endothermic phase transitions were observed around 313, 333, 373 and 393 K. These phase transitions correspond to melting of the PEO domain (~313 K), melting of the azobenzene moieties (~333 K), the liquid-crystalline transition from smectic C to smectic A (~373 K, indicated by an arrow in the inset) and the isotropic transition (~393 K) (Yoshida *et al.*, 2004; Watanabe *et al.*, 2006). With increasing $LiCF_3SO_3$ concentration the endothermic peak of the PEO melting decreased and disappeared above $f_{Li} = 1.3 \times 10^{-1}$. $LiCF_3SO_3/PEO_{114}$-b-$PMA(Az)_{51}$ above $f_{Li} = 2.5 \times 10^{-1}$ had a new endothermic peak around 433 K. This temperature is similar to the melting temperature of complexes of PEO with $LiCF_3SO_3$ (Rhodes & Frech, 2001). According to their report, one $LiCF_3SO_3$ forms a complex with three ethylene oxide (EO) units in the $PEO/LiCF_3SO_3$ complex. $LiCF_3SO_3/PEO_{114}$-b-$PMA(Az)_{51}$ with $f_{Li} = 2.5 \times 10^{-1}$, in which the number of PEO repeating units per $LiCF_3SO_3$ was four, gave the largest fusion enthalpy of all the $LiCF_3SO_3/PEO_{114}$-b-$PMA(Az)_{51}$ complexes, therefore the endothermic peak of $LiCF_3SO_3/PEO_{114}$-b-$PMA(Az)_{51}$ with $f_{Li} = 2.5 \times 10^{-1}$ and 1.0 observed around 433 K was assigned as melting of the $LiCF_3SO_3/PEO$ complex in the $LiCF_3SO_3/PEO_{114}$-b-$PMA(Az)_{51}$ system. The melting peak of the $LiCF_3SO_3/PEO$ complex in $LiCF_3SO_3/PEO_{114}$-b-$PMA(Az)_{51}$ with $f_{Li} = 1$ was broad and small. This fact suggested that the excess amount of $LiCF_3SO_3$ disturbed the crystallization of the $PEO/LiCF_3SO_3$ complex. Below $f_{Li} = 1.3 \times 10^{-1}$,
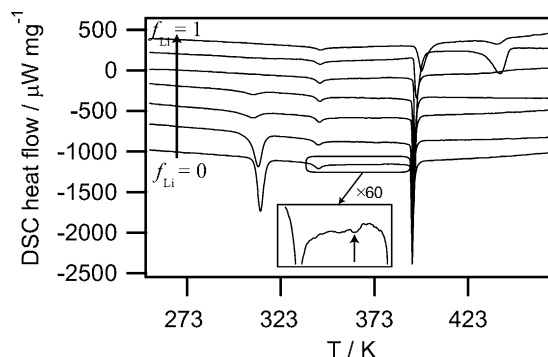
Figure 2
DSC heating curves of PEO_{114}-b-$PMA(Az)_{51}$ ($f_{Li} = 0$, bottom) and $LiCF_3SO_3/PEO_{114}$-b-$PMA(Az)_{51}$ systems with $f_{Li} = 8.3 \times 10^{-3}$, 2.5×10^{-2}, 5.0×10^{-2}, 1.3×10^{-1}, 2.5×10^{-1} and 1.0 from bottom to top.

in which the number of PEO repeating units per LiCF$_3$SO$_3$ was more than 20, the melting peak of PEO in the LiCF$_3$SO$_3$/PEO$_{114}$-b-PMA(Az)$_{51}$ systems became broad and small with increasing LiCF$_3$SO$_3$ concentration. The existence of a small amount of LiCF$_3$SO$_3$ relative to the PEO repeating unit inhibited the crystallization of the PEO domain in PEO$_{114}$-b-PMA(Az)$_{51}$. The molar equivalent was important for forming crystals of PEO/LiCF$_3$SO$_3$ complex.

On the other hand, phase transitions concerning the hydrophobic PMA(Az) domain in PEO$_{114}$-b-PMA(Az)$_{51}$ showed different tendencies with LiCF$_3$SO$_3$ concentration. Both the melting of azobenzene moieties and the isotropic transition were scarcely influenced by the addition of LiCF$_3$SO$_3$ for the LiCF$_3$SO$_3$/PEO$_{114}$-b-PMA(Az)$_{51}$ systems below f_{Li} = 5.0 × 10^{-2}. However, in the case of f_{Li} = 1.3 and 2.5 × 10^{-1}, the isotropic transition temperature (T_{Iso}) and enthalpy (ΔH_{Iso}) shifted slightly to higher temperatures and decreased compared with the isotropic transition of PEO$_{114}$-b-PMA(Az)$_{51}$ (f_{Li} = 0). The solid PEO/LiCF$_3$SO$_3$ complex in the PEO domain, having a higher melting temperature than T_{Iso}, reduced the molecular mobility of the PMA(Az) domain in the isotropic state, therefore T_{Iso} increased. The decrease of ΔH_{Iso} indicated the restricted molecular motion of the liquid-crystalline parts by the solid PE/LiCF$_3$SO$_3$ complex and disorder in the smectic layer of the PMA(Az) domain.

3.2. Nanostructures

3.2.1. PEO$_{114}$-b-PMA(Az)$_{51}$. Fig. 3 shows SAXS profiles of PEO$_{114}$-b-PMA(Az)$_{51}$ (f_{Li} = 0) at room temperature and 423 K (isotropic state). The nanostructure at room temperature was assigned as the hexagonally packed PEO cylinder structure, because the ratio of each diffraction peak to the first-order peak (q*) was q*: $(3q*)^{0.5}$: $(4q*)^{0.5}$: $(7q*)^{0.5}$. At q = 2.0 nm^{-1}, another peak corresponding to smectic layers of PMA(Az) domains was observed at room temperature. At 423 K, where the PMA(Az) domain was in the isotropic state, the peak coming from the smectic layers disappeared. On the other hand, three peaks, shown by arrows in Fig. 3, were observed, although these peak intensities were much weaker than those at room temperature. Since the ratios of the diffraction peaks were q*: $(2q*)^{0.5}$: $(3q*)^{0.5}$, the nanostructure at 423 K was assigned as having a body-centered-cubic (b.c.c.) structure. The hexagonally packed PEO cylinder structure of PEO$_{114}$-b-PMA(Az)$_{51}$ changed to the b.c.c. structure at the isotropic transition.
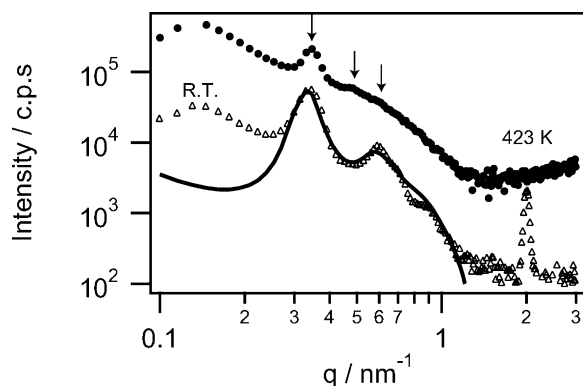
Figure 3
SAXS profiles of PEO$_{114}$-b-PMA(Az)$_{51}$ obtained at room temperature (R.T., triangles) and 423 K (filled circles). Arrows: peak positions at 423 K. Solid line: best-fit result from equation (1).

The radius of the PEO cylinder (R) was estimated by the paracrystal model (Hashimoto *et al.*, 1994). In this model, the observed scattering intensity from a hexagonally packed cylinder structure having a random orientation [$I(q)$] is given by

$$I(q) = q^{-1}I_\perp(q), \tag{1}$$

where $I_\perp(q)$ is a scattering function having uniaxial orientation. $I_\perp(q)$ is given by

$$I_\perp(q, \phi) = \frac{1}{2\pi}\int_0^{2\pi} \langle f^2 \rangle - |\langle f \rangle|^2 + |\langle f \rangle|^2 Z \, d\phi, \tag{2}$$

where f and Z indicate the form factor and the structure factor, respectively. The form factor $f(q)$ is given by

$$f(q) = C\frac{J_1(qR)}{qR}\exp\left(-\frac{q^2\sigma_s^2}{2}\right), \tag{3}$$

$$\langle f^n \rangle = \frac{\int_0^\infty P(R)f^n(q, R) \, dR}{\int_0^\infty P(R) \, dR}, \tag{4}$$

$$P(R) \simeq \exp\left[-\frac{(R - \overline{R})^2}{2\sigma_R^2}\right], \tag{5}$$

where C is a constant including the electron density difference and scattering volume, J_1 is the first-order Bessel function, R is the radius of the cylinder, $\overline{R}$ is the mean radius, σ_R is the standard deviation of R and σ_s is the characteristic thickness of a interface. σ_s is related to the thickness of the interface between each domain (t) by $t/(2\pi)^{0.5}$ (Shibayama & Hashimoto, 1986). The structure factor Z is given by

$$Z = Z_1 Z_2, \tag{6}$$

$$Z_1 = \{q - \exp[-(\Delta^2 a)q^2 P]\}(1 - 2\exp[-(1/2)(\Delta^2 a)q^2 P] \\ \times \cos\{aq\cos[\phi - (\pi/6)]\} + \exp[-(\Delta^2 a)q^2 P])^{-1}, \tag{7}$$

$$Z_2 = \{q - \exp[-(\Delta^2 a)q^2 P]\}\{1 - 2\exp[-(1/2)(\Delta^2 a)q^2 P] \\ \times \cos[aq\sin(\phi)] + \exp[-(\Delta^2 a)q^2 P]\}^{-1} \tag{8}$$

$$P = \cos^2[\phi - (\pi/6)] + \sin^2\phi, \tag{9}$$

where a and Δa are the lattice constant of the hexagonal structure and the paracrystal distortion factor, respectively. For the profile-fitting calculation, t was fixed to 0.5 nm because the interface thickness was estimated as two or three repeating units of PMA(Az) from the thermodynamic relationship between the isotropic transition entropy and the degree of polymerization of PMA(Az) (Yamada *et al.*, 2004). Since the effect of σ_R on the profile-fitting calculation was small, σ_R/R was also fixed to 0.05. Four fitting parameters, a, Δa, R and C, were used for the profile-fitting calculation. The best-fit results for PEO$_{114}$-b-PMA(Az)$_{51}$ are superimposed on the SAXS profile observed at room temperature in Fig. 3. The fitting results are listed in Table 1. The calculated result did not match the experimental data because the scattering from large grains overlapped in the low-q region and the intensity was not high enough in the high-q region. The PEO volume fraction (ϕ_{PEO}) was estimated using

$$\phi_{PEO} = \frac{2\pi}{3^{1/2}}\left(\frac{R}{a}\right)^2. \tag{10}$$

ϕ_{PEO} of PEO$_{114}$-b-PMA(Az)$_{51}$ was 0.06. In the case of a linear diblock copolymer having a step-function-type electron density profile, the border between the hexagonally packed cylinder structure and the b.c.c. structure is ϕ_A = 0.12, where ϕ_A is the minor component (Lodge

& Muthukumar, 1996). Although the ϕ_{PEO} value of PEO_{114}-b-$PMA(Az)_{51}$ (0.06) was lower than the border ϕ_{PEO} value between the hexagonally packed cylinder structure and the b.c.c. structure (0.12) (Lodge & Muthukumar, 1996), the hexagonally packed cylinder structure was stable at room temperature for PEO_{114}-b-$PMA(Az)_{51}$. For PEO_{114}-b-$PMA(Az)_n$, the hexagonally packed cylinder structure is stable when the PMA(Az) domain is in the smectic phase to compensate for the conformational entropy loss of the smectic phase formation by the increase of freedom in the interface between the hydrophilic and hydrophobic domains (Yoshida *et al.*, 2004). This assumption conformed to the observation of the transformation from the hexagonally packed cylinder structure to the b.c.c. structure at the isotropic transition. Anthamatten & Hammond determined phase diagrams of side-chain liquid-crystalline copolymers by theoretical calculation. When the side-chain liquid crystal took a planar anchoring on the interface between each block, the side-chain liquid-crystal copolymer preferred to form the cylinder structure over a wide range of volume fractions compared with linear block copolymers (Anthamatten & Hammond, 2001).

3.2.2. $LiCF_3SO_3$/PEO_{114}-b-$PMA(Az)_{51}$ systems. Fig. 4 shows SAXS profiles of $LiCF_3SO_3$/PEO_{114}-b-$PMA(Az)_{51}$ systems having various f_{Li} values at room temperature. In the q range between 0.1 and $1 \, nm^{-1}$, the diffraction peaks corresponding to the hexagonally packed cylinder structure were observed for all systems. The diffraction peak of the smectic layers also appeared at $q = 2 \, nm^{-1}$. Although the peak position of the smectic layers scarcely changed below $f_{Li} = 2.5 \times 10^{-1}$, the half bandwidth increased with increasing $LiCF_3SO_3$ concentration. In particular, above $f_{Li} = 1.3 \times 10^{-1}$ the smectic layer peak became broad and the position of the peak shifted to lower q for the system with $f_{Li} = 1.0$. When the $LiCF_3SO_3$ concentration was close to the molar equivalent value, the formation of the complex between three EO units and one $LiCF_3SO_3$ occurred efficiently. The complex of PEO/$LiCF_3SO_3$ acted as a cross linkage between the PEO chains and decreased the molecular mobility of the PEO. Then the hydrophilic PEO cylinder changed to a viscous cylinder and induced disordering of the smectic layers in the hydro-
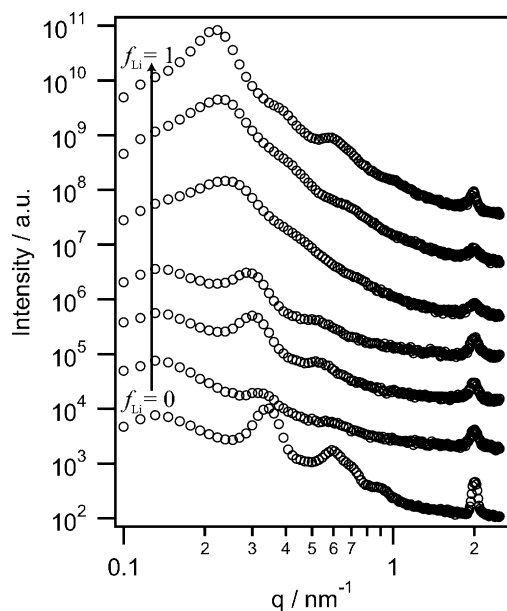
Figure 5
Typical fitting results for $LiCF_3SO_3$/PEO_{114}-b-$PMA(Az)_{51}$ systems with $f_{Li} = 2.5 \times 10^{-1}$ (top) and 1.0 (bottom) at room temperature.

phobic PMA(Az) domain. The SAXS experiment results showed a good agreement with the DSC results shown in Fig. 2.

The nanostructures of $LiCF_3SO_3$/PEO_{114}-b-$PMA(Az)_{51}$ were evaluated by SAXS profile fitting using equation (1). The fitted results for $LiCF_3SO_3$/PEO_{114}-b-$PMA(Az)_{51}$ systems with $f_{Li} = 2.5 \times 10^{-1}$ and 1.0 are shown in Fig. 5, and the values obtained are listed in Table 1. These fitted results also did not match the experimental results in the low-q region for the same reason as for PEO_{114}-b-$PMA(Az)_{51}$ ($f_{Li} = 0$). Since the PEO complexes with $LiCF_3SO_3$ had a larger volume than PEO, the radius of the PEO cylinder (R) increased with increasing $LiCF_3SO_3$ concentration. Concurrently, $LiCF_3SO_3$ acted as a cross-linker between the PEO chains and restricted the molecular motion of the PEO, therefore the disorder ($\Delta a/a$) also increased with increasing $LiCF_3SO_3$ concentration.

Fig. 6 shows SAXS profiles for the $LiCF_3SO_3$/PEO_{114}-b-$PMA(Az)_{51}$ systems with $f_{Li} = 2.5 \times 10^{-2}$ ($\phi_{PEO} = 0.09$) and $f_{Li} = 1$ ($\phi_{PEO} = 0.23$) at 423 and 473 K, respectively, where both systems are in the isotropic state. The nanostructure of the system with $f_{Li} = 2.5 \times 10^{-2}$ in the isotropic state was the b.c.c. structure, the same as that of PEO_{114}-b-$PMA(Az)_{51}$ at 423 K (Fig. 2). The ϕ_{PEO} values of the $LiCF_3SO_3$/PEO_{114}-b-$PMA(Az)_{51}$ systems used in this study, from 0.06 to 0.23 as shown in Table 1, covered the border ϕ_{PEO} value (0.12) between the hexagonally packed cylinder structure and the b.c.c. structure expected by theoretical calculations for linear block copo-

Figure 4
SAXS profiles of PEO_{114}-b-$PMA(Az)_{51}$ ($f_{Li} = 0$, bottom) and $LiCF_3SO_3$/PEO_{114}-b-$PMA(Az)_{51}$ systems with $f_{Li} = 8.3 \times 10^{-3}$, 2.5×10^{-2}, 5.0×10^{-2}, 1.3×10^{-1}, 2.5×10^{-1} and 1.0 from bottom at room temperature.
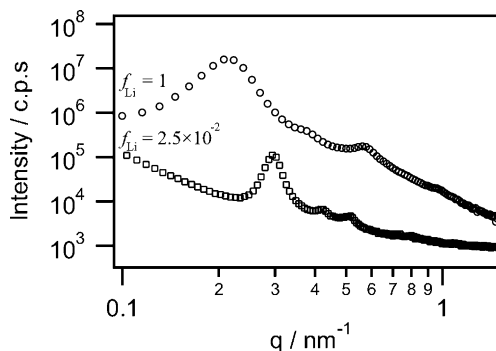
Figure 6
SAXS profiles of $LiCF_3SO_3$/PEO_{114}-b-$PMA(Az)_{51}$ systems in the isotropic state. Open circles: $f_{Li} = 1$ at 473 K; open squares: $f_{Li} = 2.5 \times 10^{-2}$ at 423 K.

lymers (Lodge & Muthukumar, 1996). Therefore, the nanostructure of the system with $f_{Li} = 1.0$ was the hexagonally packed cylinder structure in the isotropic state, because $\phi_{PEO} = 0.23$ was larger than the border value. These results also indicated that $LiCF_3SO_3$ increased ϕ_{PEO} of the $LiCF_3SO_3/PEO_{114}$-b-$PMA(Az)_{51}$ systems by the formation of an $LiCF_3SO_3/PEO$ complex.

4. Conclusion

Phase transitions and nanostructures of $LiCF_3SO_3/PEO_{114}$-b-$PMA(Az)_{51}$ systems were investigated by DSC and SAXS. The $LiCF_3SO_3/PEO_{114}$-b-$PMA(Az)_{51}$ systems above $f_{Li} = 2.5 \times 10^{-1}$, which corresponds to four PEO repeating units per $LiCF_3SO_3$ molecule, formed a complex of $LiCF_3SO_3/(EO)_3$. The complex of $LiCF_3SO_3/PEO$ melted at 433 K, which was higher than the isotropic transition of the PMA(Az) domain. The addition of $LiCF_3SO_3$ induced disordering in the PEO_{114}-b-$PMA(Az)_{51}$ nanostructure and the liquid-crystal structure due to the molecular motion of the PEO domains being restricted by the complex formation. On the other hand, the addition of $LiCF_3SO_3$ increased the radius of the PEO cylinder and the volume fraction of the PEO domain. The structure transition from the hexagonally packed cylinder to the b.c.c. structure occurred for $LiCF_3SO_3/PEO_{114}$-b-$PMA(Az)_{51}$ with $f_{Li} = 2.5 \times 10^{-2}$ ($\phi_{PEO} = 0.09$) in the isotropic state, but not for $LiCF_3SO_3/PEO_{114}$-b-$PMA(Az)_{51}$ with $f_{Li} = 1.0$ ($\phi_{PEO} = 0.23$).

References

Anthamatten, M. & Hammond, P. T. (2001). *J. Polym. Sci. B*, **39**, 2671–2691.

Arai, A.A., Morita, T. & Nishikawa, K. (2003). *J. Chem. Phys.* **119**, 1502–1509.

Hamley, I. W. (1998). *The Physics of Block Copolymers*. New York: Oxford University Press.

Hamley, I. W. & Castelletto, V. (2004). *Prog. Polym. Sci.* **29**, 909–948.

Hashimoto, T., Kawamura, T., Harada, M. & Tanaka, H. (1994). *Macromolecules*, **27**, 3063–3072.

Jung, S., Yamada, T., Iyoda, T. & Yoshida, H. (2005). *J. Therm. Anal. Cal.* **81**, 563–567.

Jung, S. & Yoshida, H. (2006). *J. Therm. Anal. Cal.* **85**, 719–724.

Kato, T., Minewaki, K., Kawabata, Y., Imai, M. & Takahashi, Y. (2004). *Langmuir*, **20**, 3504–3508.

Kawabata, Y., Nagao, M., Seto, H., Komura, S., Takeda, T., Schwahn, D., Yamada, N. L. & Nobutou, H. (2004). *Phys. Rev. Lett.* **92**, 056103–056106.

Lazzari, M. & López-Quintela, M. A. (2003). *Adv. Mater.* **15**, 1583–1594.

Lemmich, J., Mortensen, K., Ipsen, J. H., Hønger, T., Bauer, R. & Mouritsen, O. G. (1996). *Phys. Rev. E*, **53**, 5169–5180.

Li, J., Kamata, K., Yamada, T., Yoshida, H. & Iyoda, T. (2005). *Polym. Prepr. Jpn*, **53**, 3N03.

Lodge, T. P. & Muthukumar, M. (1996). *J. Phys. Chem.* **100**, 13275–13292.

Rhodes, C. P. & Frech, R. (2001). *Macromolecules*, **34**, 2660–2666.

Shibayama, M. & Hashimoto, T. (1986). *Macromolecules*, **19**, 740–749.

Tian, Y., Watanabe, K., Kong, X., Abe, J. & Iyoda, T. (2002). *Macromolecules*, **35**, 3739–3747.

Tominaga, Y., Izumi, Y., Kwak, G., Asai, S. & Sumita, M. (2003). *Macromolecules*, **36**, 8766–8772.

Watanabe, R., Iyoda, T., Yamada, T. & Yoshida, H. (2006). *J. Therm. Anal. Cal.* **85**, 713–717.

Yamada, T., Watanabe, R., Watanabe, K., Koyanagi, C., Yoshida, H. & Iyoda, T. (2004). *Polym. Prepr. Jpn*, **53**, 1089.

Yamada, T., Yoshii, T., Ozawa, N., Kawabata, Y., Kato, T. & Yoshida, H. (2005). *Trans. Mater. Res. Sci. Jpn*, **30**, 675–678.

Yoshida, H., Kinoshita, R. & Teramoto, Y. (1995). *Thermochim. Acta*, **264**, 173–183.

Yoshida, H., Watabane, K., Watanabe, R. & Iyoda, T. (2004). *Trans. Mater. Res. Sci. Jpn*, **29**, 861–864.